C. R. Physique 3 (2002) 79–88

Électromagnétisme, optique/*Electromagnetism, optics*
(Solides, fluides : propriétés électroniques et optiques/*Solids, fluids: electronic and optical properties*)

DOSSIER

MICROCAVITÉS ET CRISTAUX PHOTONIQUES
MICROCAVITIES AND PHOTONIC CRYSTALS

Metallic photonic crystals

Jean-Michel Lourtioz *, André de Lustrac

Institut d'électronique fondamentale, université Paris XI, URA 22 du CNRS, bât 220, 91405 Orsay, France

Received and accepted 23 November 2001

Note presented by Guy Laval.

Abstract Metallic photonic crystals (PC), also originally called artificial dielectrics, have properties different from those of their dielectric homologues. They are of strategic interest for the microwave domain where they exhibit sufficiently weak loss in addition to their robustness, conformability and low-cost fabrication. In this paper, we review some recent results on metallic photonic crystals and their potential applications to microwave circuits and antennas. After recalling spectral properties of metallic PC, we successively address ultra-compact structures such as high-impedance surfaces, electrically controllable photonic band gaps and left-handed materials. Finally, we discuss new opportunities offered by metallic PCs in the optical domain. To cite this article: J.-M. Lourtioz, A. de Lustrac, C. R. Physique 3 (2002) 79–88. © 2002 Académie des sciences/Éditions scientifiques et médicales Elsevier SAS

photonic bandgap materials / microstructures / microwaves / optics

Les cristaux photoniques métalliques

Résumé Les cristaux photoniques métalliques, aussi appelés diélectriques artificiels à leur origine, ont des propriétés différentes de celles de leurs homologues diélectriques. Ils sont d'intérêt stratégique pour le domaine des micro-ondes où ils présentent des pertes suffisamment faibles, associées à leur robustesse, leur conformité et leur faible coût. Dans cet article, nous faisons une revue de résultats récents sur les cristaux photoniques métalliques et leurs applications potentielles aux circuits et antennes micro-ondes. Après avoir rappelé les propriétés spectrales des cristaux photoniques métalliques, nous discutons successivement des structures ultra-compactes comme les surfaces à haute impédance, des bandes interdites photoniques contrôlables électriquement et des matériaux à indice de réfraction négatif. Enfin, nous discutons d'opportunités nouvelles offertes par les cristaux photoniques métalliques dans le domaine optique. Pour citer cet article : J.-M. Lourtioz, A. de Lustrac, C. R. Physique 3 (2002) 79–88. © 2002 Académie des sciences/Éditions scientifiques et médicales Elsevier SAS

matériaux à bandes interdites photonique / microstructures / micro-ondes / optique

* Correspondence and reprints.
E-mail address: jean-michel.lourtioz@ief.u-psud.fr (J.-M. Lourtioz).

S1631-0705(02)01293-8/FLA

1. Introduction

One-, two- and three-dimensional (1D, 2D, 3D) periodic ensembles of metallic elements have been proposed as early as in the beginning of the last century to create artificial dielectrics with fully controllable dielectric permittivity in the microwave domain [1]. Indeed, these artificial media were nothing else than photonic crystals (PC), but severe difficulties in terms of technology, modelling and measurements limited their potential applications in these early times. For instance, the large structure sizes a priori imposed by the half-wavelength periodicity appeared to be prohibitive for many radar and antenna applications in the long-wavelength range ($\lambda \sim 1$ m).

Several decades were needed to renew a tremendous interest for photonic crystals with the experimental demonstration of a full photonic band gap (PBG) by E. Yablonovitch and his co-workers in 1991 [2]. Since that time, studies have no longer been limited to the low-frequency region of the electromagnetic spectrum, but have covered a very wide spectral range from microwaves to optics [3]. Either dielectric, metallic or metallo-dielectric structures have been considered. Metallic PCs have been preferred for the microwave domain where they exhibit sufficiently weak loss in addition to their robustness, conformability and low-cost fabrication. Unlike previous works on 'artificial dielectrics', a considerable effort has been made to reduce the structure sizes in the long wavelength range. One of the most decisive progresses in that direction has been the development of high-impedance surfaces and ultra-compact photonic band gaps (UCPBG) for both antenna and microwave circuit applications [4–8]. Another important progress has been the experimental demonstration of active or controllable PBGs with the insertion of electronic devices in the structures [9,10]. More recently, periodic metallic structures combining nonmagnetic split ring resonators and continuous wires have also been used to fabricate new composite materials that simultaneously exhibit negative permeability and permittivity [11,12]. 'Perfect superlenses' have been proposed to exploit this new type of materials [13]. In the same time, the fabrication of metallic PCs at optical wavelengths has been investigated with different techniques [14,15]. One of the objectives in that domain being the enhancement of light emission using surface-plasmon resonances [16–18].

Following this brief historical review, the properties of metallic PCs are discussed with more detail in the rest of the paper. Sections 2–5 are devoted to metallic PCs in the microwave domain. The spectral characteristics of metallic PCs are compared to their dielectric homologues in Section 2. High-impedance surfaces and ultra-compact PCs for microwave applications are presented in Section 3. Electrically controllable PCs are shown with their first applications to antennas in Section 4. New composite materials with negative index of refraction are introduced in Section 5. Finally, Section 6 is related to metallic PCs in the optical domain. Some aspects related to their fabrication and their future developments are discussed. This is followed by a general conclusion in Section 7.

2. Spectral characteristics of standard metallic PCs in the microwave domain

Unlike dielectrics, currents can propagate into metals. However, surface currents penetrate only a very small distance at microwave frequencies. For example, the skin depth, defined as: $\delta = \sqrt{2/\omega\mu_0\sigma}$ with σ being the metal conductivity [1], is less than one micron for copper at 10 GHz. The electromagnetic energy thus tends to be expulsed out from the material. On the other hand, microwave frequencies are far below the plasma frequency and the effective dielectric constant of a metal in the microwave domain can be expressed as: $\varepsilon = 1 - j\sigma/\omega\varepsilon_0$, where σ is real [1].

Because of these material properties, metallic PCs exhibit a quite different spectral behaviour as compared to dielectric PCs. This is illustrated in Fig. 1, which shows the transmission spectrum of a 2D dielectric PC (a) and that of a 2D metallic PC (b) with a similar lattice geometry. The dielectric PC consists of a square lattice of 10 mm long alumina rods ($\varepsilon \sim 9$) with a lattice periodicity $a = 3$ mm and a rod diameter $d = 1.5$ mm. The metallic PC is a square lattice of 5 mm copper rods with a lattice periodicity $a = 6$ mm and a rod diameter $d = 2$ mm. In each figure, both measurements and calculations are reported. The microwave setup used for the measurements consisted of a vectorial network analyser HP 8510C

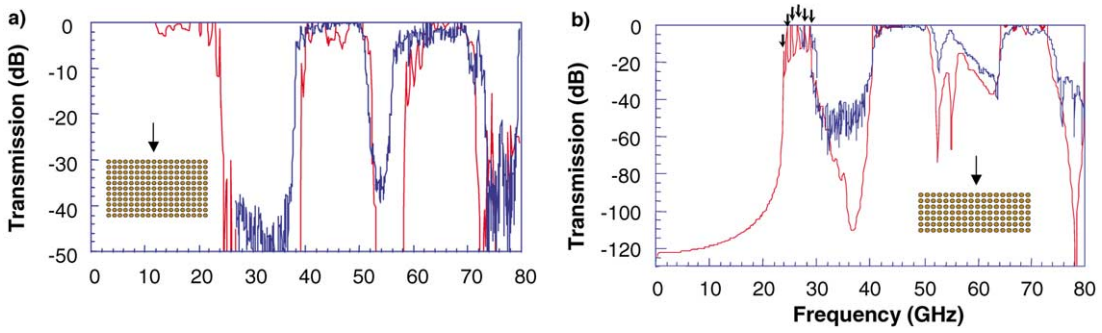

Figure 1. Transmission spectra of square lattices of rods for a normal incidence and a TM polarization. (a) The lattice comprises 11 rows of 18 alumina rods with a 3 mm period and a 1.5 mm rod diameter. (b) The lattice comprises 7 rows of 18 copper rods with a 6 mm period and a 2 mm rod diameter. In (a) and (b), the thin (red) curves are the calculations while the thicker (blue) curves are the measurements.

connected to two identical horns. Transmission measurements were performed at a normal incidence, for a TM field polarization (electric field parallel to the rods) and over a frequency range from 25 to 80 GHz. The microwave beam was collimated (≈ 3 cm width at 50 GHz) and absorbing foam was used to eliminate off axis parasitic waves diffracted by the crystal. The noise floor with an absorbing block between the antennas was around -45 dB. The numerical simulations were performed with proprietary finite difference time domain (FDTD) software. A pulsed plane-wave was injected onto the PC, a virtual diaphragm being placed at the PC entrance to account for the finite width of the microwave beam. We assumed rods of infinite length as well as a lossless metal. The calculated transmission was taken as the ratio between the output and input field intensities on the beam axis. The transmission spectra were obtained after applying a fast Fourier transformation.

The first photonic gap of the dielectric PC (Fig. 1a) approximately occurs for the Bragg condition: $\lambda/2 \sim a$ in the crystal. The corresponding frequency is $\omega \sim c/2n_{\text{eff}}a$, where n_{eff} is the effective refractive index defined in the low frequency range. Indeed, we check that for a dielectric filling factor $f \sim 0.2$, the effective medium permittivity is $\varepsilon_{\text{eff}} = (1-f) + f\varepsilon \sim 2.6$ leading to $n_{\text{eff}} = \sqrt{\varepsilon_{\text{eff}}} \sim 1.6$ and $\omega \sim 31.5$ GHz in excellent agreement with both FDTD calculations and measurements. The situation is quite different for the metallic PC (Fig. 1b). The first photonic gap starts from the zero frequency. Within this gap, metallic PCs behave like bulk metals near the plasma resonance [21,22] and the attenuation is much stronger than that observed in the gaps of dielectric PCs. This band is followed by the first transmission band for $\lambda/2 \sim a$ (just the opposite of what is observed for dielectric PCs). The metallic PC then behaves as an ensemble of identical coupled Fabry–Perot cavities in the field propagation direction. In the case of Fig. 1b, six cavities are present leading to six allowed modes in the transmission band. The band centre (27 GHz) is close to the value calculated from $\omega = c/2a$ (25 GHz). This band is then followed by a succession of other forbidden and transmission bands, whose contrast becomes less pronounced at higher frequencies. It is worthwhile noting the good agreement between calculations and measurements over the whole frequency range of measurements. The same study has been carried out for the TE polarization (electric field perpendicular to the rows). For 2D PCs of disconnected rows, the TE photonic gaps are known to be less pronounced than the TM ones [3]. However, metallic PCs present the strongest polarization dependence.

3. High-impedance surfaces and ultra-compact PBGs

The main drawback of standard metallic PCs shown in Section 2 is the large volume they occupy. Planar devices are preferred in many applications and the search for compact metallic PCs is of strategic importance in the microwave domain [4–8]. In turn, if the periodic corrugations defining the metallic PC are

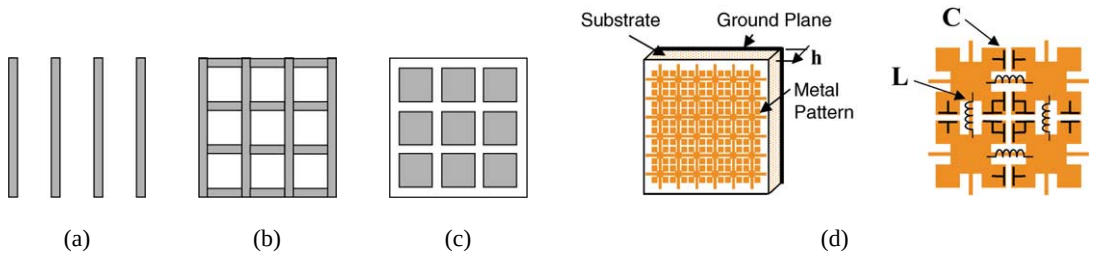

Figure 2. From metallic grids to ultra-compact photonic band gaps (UCPBG). (a) One-dimensional inductive grid. (b) Two-dimensional inductive grid. (c) Two-dimensional capacitive grid. (d) Left: UCPBG obtained by a Jerusalem cross patterning of a substrate ground plane; right: equivalent circuit of the UCPBG unit cell.

small compared to the wavelength, their electromagnetic properties can be described using lumped circuit elements – capacitors and inductors. For example, let us consider the one-dimensional grids of thin parallel wires that usually constitute the individual layers of standard PCs (Fig. 2a). They are known to block the TM field polarization due to inductive coupling between wires. Both the grid elements and the grid itself can be represented as pure inductances for wavelengths larger than the grid period [21]. Inductive couplings are also present in two-dimensional wire meshes (Fig. 2b) that block both TE and TM polarizations and behave as high-pass filters for. In contrast, the dual system consisting of 2D periodic metallic patches (Fig. 2c) involves capacitive couplings and behaves as a low-pass filter.

The basic idea of ultra-compact PBGs and high-impedance surfaces is to combine both inductive and capacitive effects. A rejection band (i.e., an electromagnetic band gap) can then be achieved for frequencies around the resonance frequency ω_0 defined as: $LC\omega_0^2 = 1$. One example of UCPBG is shown in Fig. 2d (left). The metallic ground plane of a planar waveguide is periodically etched following a Jerusalem cross pattern [7,8]. The equivalent circuit corresponding to the unit cell is represented in Fig. 2d (right) with inductances and capacitors. Several applications to microwave circuits have been proposed including both coplanar and microstrip filters for high-gain amplifiers [7,8]. The high effective permittivity attained near the electromagnetic gap allows the use of compact devices. Fig. 3 shows a band pass filter with 2ω-rejection, fabricated by structuring both the metallic ground plane and the dielectric waveguide layer [22]. The filtering at ω is achieved using $\lambda/2$ resonators while the second-harmonic rejection results from a ground plane PBG. The maximum transmission can reach -3 dB for a ~ 12 dB contrast ratio between ω and 2ω frequencies. Such a filter is 20% more compact than conventional systems with similar performances.

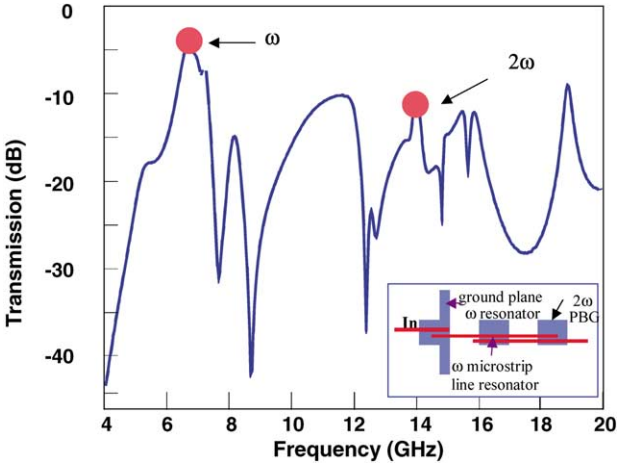

Figure 3. Measured transmission spectrum (S21 parameter) of a compact planar two-pole filter with second-harmonic rejection. The filtering at ω is achieved using $\lambda/2$ microstrip resonators while the second-harmonic rejection results from a ground plane PBG. A schematic view of the filter is shown in the insert.

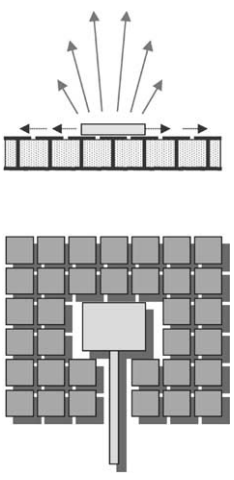

(a)

(b)

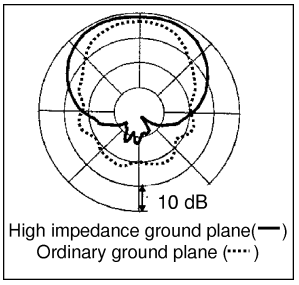

Figure 4. (a) Cross section and top view of a patch antenna on a high-impedance surface. The main antenna emission (vertical arrows) is enhanced while surface waves (horizontal arrows) are suppressed. (b) Measured radiation patterns of an antenna placed either on a high impedance ground plane or an ordinary ground plane [23].

High-impedance surfaces are more specifically dedicated to antenna applications. Fig. 4 (left) shows a schematic view of the structure developed by Sievenpiper et al. [23,24]. A capacitive grid of metallic patches is fabricated on a dielectric substrate. Inductances are created with metallic vias connecting the patch elements to the substrate ground plane. The via length and thus, the substrate thickness can be chosen much smaller than the operating wavelength. The impedance of such a structure is that of a parallel resonant LC circuit given by: $Z = jL\omega/(1 - LC\omega^2)$. Near resonance, the impedance is very high such that currents on the surface radiate very efficiently, and the structure suppresses the propagation of all types of surface waves (TM and TE). Having high surface impedance, it also reflects external electromagnetic waves without the phase reversal that occurs on a flat conductor. This allows a radiating element to be directly adjacent to the surface (Fig. 4, left). In other words, the direction of the image currents results in constructive, rather than destructive interference, allowing an antenna to radiate efficiently. Furthermore, in the forbidden frequency band, the high-impedance structure does not support freely propagating surface currents, resulting in an improved radiation pattern. Fig. 4 (right) shows the radiation patterns of a patch antenna when it is placed either on a high impedance ground plane or an ordinary ground plane [23]. Using the high impedance ground plane, the backward emission is strongly reduced leading to a more efficient antenna.

4. Electrically controllable photonic crystals

The use of metallic structures allows an easy insertion of electrically active elements into PCs. This was at the origin of the active PC concept first proposed by two French groups in Orsay and Lille, respectively [10]. Electrically controllable PCs have been obtained by inserting p–i–n diodes along the metallic wires or stripes of a 2D crystal lattice. When the diodes are on, the crystal properties are close to those of a PC with continuous metallic wires. When the diodes are off, a tight analogy exists with a photonic crystal consisting of discontinuous metallic wires and dielectric inserts: A transmission (valence) band appears instead of the plasmon-like band [25].

Actually, a p–i–n diode can be approximated by an equivalent circuit including a capacitor and a resistor in parallel. The PC behaviour will thus depend on the respective values of the resistor and the capacitor. Fig. 5 shows the transmission spectra calculated in the two extreme cases for a 2D active PC in the printed circuit technology. The incident field is TM polarized. Fig. 5a corresponds to the situation where the capacitor has the dominant influence (infinite value for the resistor). As expected, the first forbidden band is

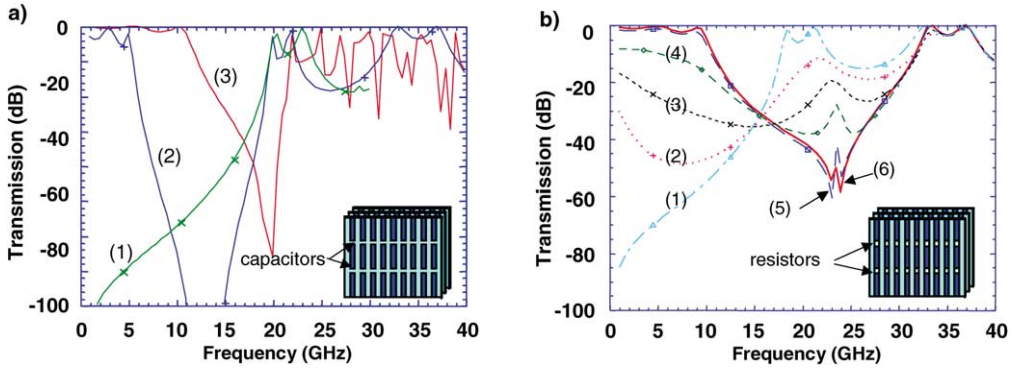

Figure 5. Calculated transmission spectra of metallic wire photonic crystals with capacitors (a), or resistors (b), periodically inserted along the wires. Three-layer crystals are shown in the inserts. The layers (printed boards) are separated by 6 mm. In each layer, the distance between neighbouring metallic stripes is 4 mm and the distance between two consecutive capacitors (or resistors) along the same wire is 5 mm (4.5 mm). In (a), curves (1), (2) and (3) correspond to capacitor values of 0, 0.3 and 30 fF, respectively. In (b), curves (1) to (6) correspond to resistor values of 0, 50, 150, 500, 5000 and 15 000 Ω, respectively.

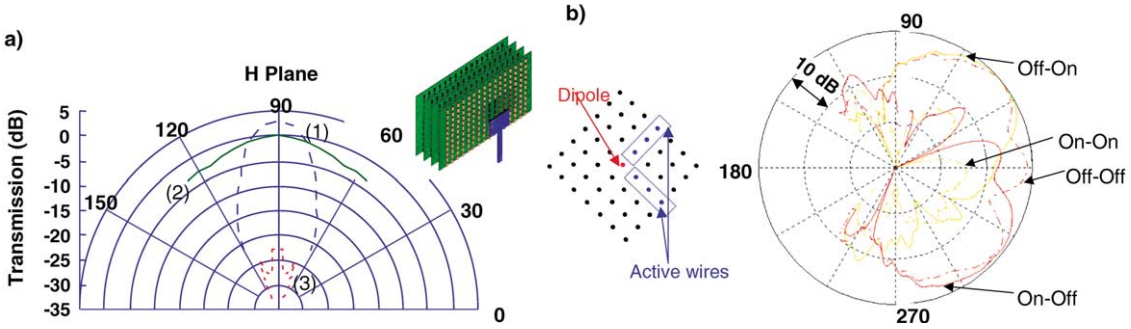

Figure 6. (a) Patch antenna with active PC radome (upper right). Measured radiation patterns for the patch antenna alone (broad lobe (2)), with the radome in the transmission state (narrow lobe (1)) and with the radome in the reflection state (30 dB attenuation (3)). (b) Schematic view of a 2D metallic PC with two series of active wires (left). A dipolar antenna is placed at the PC centre. Various radiation patterns obtained by modifying the states of the two series of active elements (right).

replaced by a transmission band whose edge is shifted toward higher frequencies for increasing capacitance values. The rest of the spectrum is not modified. A quite different behaviour is observed when the resistor has the dominant influence (Fig. 5b). Not only the first band but also higher order bands are strongly modified. The smaller the resistor, the stronger the modifications. All these numerical predictions from a FDTD model have been confirmed in recent experiments [9,26]. The PC was continuously tuned from a transmission state to a reflection state by varying the diode bias (i.e., by varying the diode resistance).

Electrically controllable PCs can be used as active radomes or spatial filters to control the radiation patterns of antennas. Two works have recently been carried out in that direction. Fig. 6a shows experimental results obtained on an active radome with a patch antenna [27]. The radome is composed of three printed boards with p–i–n diodes soldered at regular intervals along parallel metallic stripes. The distance between stripes (4 mm) and that between printed boards (9 mm) are chosen to operate at $\sim$ 12 GHz on the low-frequency side of the first transmission band. The radome is placed close (1 cm) to the patch antenna to reduce leaky waves on each side of the structure and improve the matching between the PC and the antenna. As seen in Fig. 6a, the antenna radiation pattern is totally controlled with the active radome.

When the diodes are on (transmission state), the antenna is very directive. A 3 dB gain is obtained in the forward direction. When the diodes are off (reflection state), the antenna radiation is attenuated by ~ 30 dB. Fig. 6b shows other experimental results on antenna beam switching [28]. Unlike the previous scheme, a dipolar antenna is inserted in a 2D metallic wire PC with a square lattice (left view). The crystal and dipole dimensions are chosen to operate near 2 GHz within the first photonic gap. Only a few wires are active and placed in two perpendicular rows that are used as two independent waveguides. When all the active elements are on, the PC is opaque. The antenna just weakly radiates outside of the PC. When one series of active elements is off (on–off and off–on states), the antenna emission is transmitted through only one waveguide. A simultaneous switching of the two series of active elements then allows the switching of the antenna beam. Finally, when all the active elements are off, the antenna radiation is transmitted by the two waveguides, and a wide emission lobe is emitted. These results are very promising for the development of low-cost antennas with multidirectional properties.

5. Left-handed materials

In 1996, J.B. Pendry and co-workers showed that a lattice of metallic wires presents a negative permittivity in the plasmon-like band [21]. In 1999, the same authors proposed the fabrication of a negative permeability material using a periodic lattice of metallic Swiss rolls [11], the negative permeability being attained within a frequency band determined by the geometrical lattice parameters. Then, the idea came to combine the two types of lattice into a single one such that the region of negative permittivity overlaps with that of negative permeability. Several years earlier, V.G. Veselago had predicted very new properties for this so-called left-handed material [29]. Indeed, the set formed by the three vectors $\boldsymbol{E}$, $\boldsymbol{H}$ and $\boldsymbol{k}$ is a left hand set (insert of Fig. 7). Phase velocity and group velocity have opposite signs. An incident electromagnetic wave on the material is refracted following the Snell–Descartes law with a negative optical index for the material. Doppler effects are inverted.

Left-handed PCs have been demonstrated for the first time by D.R. Smith et al. in 2000 [12]. Similar structures have recently been studied by the group of Orsay.[1] The left-handed PC was fabricated using printed circuit technology. A periodic lattice of metallic stripes with a 5 mm period was printed on a first type of epoxy board. A square lattice of concentric metallic rings with the same period was printed on a second type of epoxy board. The two types of printed boards were then arranged in a 1D periodic structure such that stripes and rings appeared alternately. Two pairs of stripes and rings in succession are shown in the insert of Fig. 7. The distance between a stripe and the neighbouring rings (i.e., between two consecutive printed boards) is 2 mm. The thickness of the epoxy printed boards is 0.25 mm. The stripe width is 1 mm.

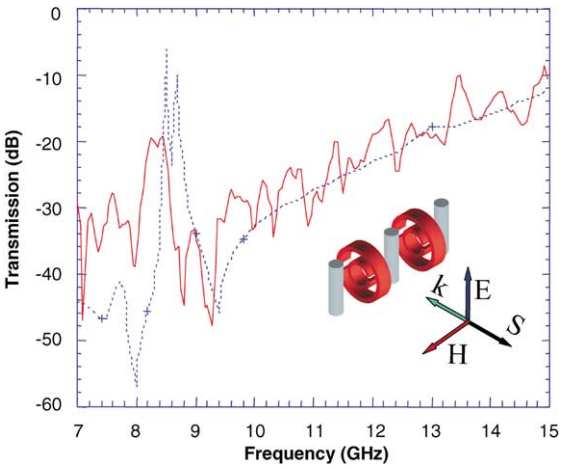

Figure 7. Measured and calculated transmission spectra of a left-handed photonic crystal (solid and dotted curves, respectively). The insert shows the basic elements of the PC (metallic stripes and pairs of concentric rings) along with the left-hand set formed by the three vectors $\boldsymbol{E}$, $\boldsymbol{H}$ and $\boldsymbol{k}$.

Each pair of concentric rings consists of an inner ring with 2 mm diameter and an outer ring with 4 mm diameter. Each ring of the pair is open and the opening width is 1 mm.

The PC transmission spectrum has been measured with the same technique as in Section 2. The incident electromagnetic wave (insert of Fig. 7) was TM polarized. Commercial finite element software (HFSS from Ansoft) was used for the numerical simulations. Fig. 7 shows the measured and calculated transmission spectra in the frequency range of interest. The average loss level is relatively high since the frequency domain corresponds to the plasmon-like band of the metallic stripe lattice. Additional losses are explained by the imperfect parallelism between printed boards. Nevertheless, a strong LC resonance occurs near 9 GHz due to the presence of the concentric rings. The two peaks are attributed to the finite number of periods in the propagation direction (three periods in our case). This is in this frequency region that both the material permittivity and permeability are negative. Indeed, a negative index of refraction has been experimentally observed around the resonance. Significant improvements in terms of loss reduction are still needed to imagine practical applications of this material at this time, but experimental results are sufficiently encouraging to stimulate further developments. The near-field control of radiating elements as well as the fabrication of 'perfect lenses' would certainly open the route to new applications [13].

6. Toward metallic photonic crystals at the optical wavelengths

Metallic mirrors are probably the most familiar optical objects in our daily life. There is no need to prove their efficiency. Metals also necessarily enter in the fabrication of electrically pumped optical devices. However, dissipative loss can limit the degree of light confinement that metals can provide at optical frequencies. Recently, the use of surface plasmon polariton (SPP) modes has been proposed to overcome the loss problem for an optical emitter close to a metallo-dielectric interface [17]. Indeed, SPP modes can propagate at the interface between a dielectric and a very thin metal layer of sub-micronic dimensions. Local-field enhancement due to surface plasmon effects has been considered in several works [18,30]. In turn, the difficulty is to efficiently couple SPP modes into a useful radiation. Several solutions for light extraction have been proposed including periodic arrays of metal particles as well as periodic and shallow corrugations on metallic layers [17]. Surface plasmon enhanced light emission of diodes has recently been reported using periodic grooves patterned on metal top layer [30]. However, further experiments are needed to confirm this result.

Perhaps a more immediate objective for metallic structures is the design of robust and wide photonic band gaps, leading to efficient frequency-selective mirrors in the infrared and visible [31]. Unlike 3D dielectric PCs, 3D metallic PCs can provide full PBG whatever the type of lattice. Two main types of 3D metallic PCs have been studied. Those consisting of connected wires present a full gap starting from zero frequency. Those consisting of disconnected spheres exhibit a gap in higher order bands. One particular difficulty is the PC fabrication itself since (sub-)micronic sizes are involved. In most cases, metallic

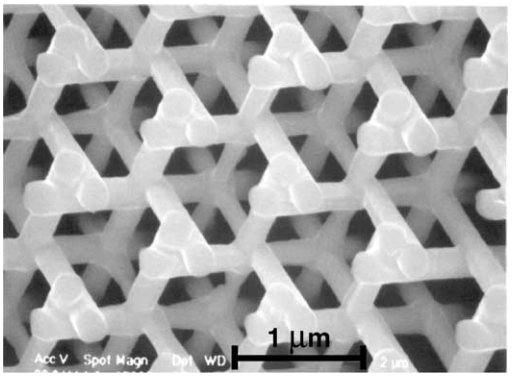

Figure 8. Scanning electron microscope image of a metallic Yablonovite obtained by copper electro-deposition in a PMMA template (top view revealing three (111) crystal planes). The XRL mask used to fabricate the template consists of a triangular lattice with a 2 µm pitch and a 500 nm hole diameter. The structure thickness is 4.3 µm. The structural integrity of the PMMA template is preserved in the metallic replicas.

elements are incorporated in a porous template. In the inverse opal technique, the template is obtained from colloidal suspensions that spontaneously form a colloidal crystal. The main drawback is the presence of stacking faults in this crystal. Another technique has recently been explored where the porous template was fabricated in a polymethyl metacrylate (PMMA) resist by X-ray lithography [15]. The Yablonovite-like metallic replica was obtained by copper electrodeposition. The resist was then removed by chemical dissolution. Fig. 8b shows a scanning electron micrograph of this metallic photonic crystal with 2 μm period and 0.5 μm wire diameter. The structure is very regular over a surface of $\sim 200 \times 200\ \mu m^2$.

7. Conclusion

We have shown that recent works on metallic photonic crystals not only can lead to new applications to microwave circuits and antennas but also directly contribute to the investigation of new physical phenomena. From a practical viewpoint, the discovery of ultra-compact photonic band gaps at long wavelengths is certainly the most decisive step toward a real application of microwave photonic crystals. UCPBG-based microwave filters have already been fabricated with excellent performances and 20% greater compactness than other existing devices. The combination of UCPBGs with active elements thus appears to be very promising for the design of new adaptative or switchable systems. From a theoretical viewpoint, the discovery of negative refractive index materials is fascinating. The near-field control of radiating elements with 'perfect lenses' at microwave frequencies raise up a strong motivation in the community even though real applications still require some efforts to reduce the material loss. One may also imagine the transposition of the left-handed material concept in the optical domain. Better control and manipulation of surface plasmons would certainly be needed for this purpose. Nevertheless, the recent fabrication of very regular 3D metallic PCs with (sub-)micronic resolution is quite encouraging for a more detailed investigation of metallic PCs in the optical domain.

[1] Djermoun A., de Lustrac A., Experimental study of negative refractive index materials at various angles of incidence, submitted for publication.

Acknowledgements. We acknowledge all the members of the French GDR on 'Microwave and microcavities' that contribute to a large part of the results presented on metallic photonic crystals.

References

[1] US patent deposited by G. Marconi and S. Franklin in 1919; A.F. Harvey, Microwave Engineering, Academic Press, London, 1963, pp. 592–605.
[2] E. Yablonovitch, T.J. Gmitter, K.M. Leung, Phys. Rev. Lett. 67 (1991) 2295.
[3] Special issue on photonic crystals, J. Opt. Soc. Am. B 10 (1993);
J. Mod. Opt. 41 (1994);
M.M. Sigalas, C.T. Chan, K.M. Ho, C.M. Soukoulis, Phys. Rev. B 52 (1995) 11744;
J.D. Joannopoulos, R.D. Meade, J.N. Winn, Photonic Crystals, Princeton University Press, Princeton, 1995.
[4] K.P. Ma, K. Hirose, F.R. Yang, Y. Qian, T. Itoh, Electron. Lett. 34 (1998) 2041–2042.
[5] D. Sievenpiper, L. Zhang, R. Broas, N. Alexopolous, E. Yablonovitch, IEEE Trans. Microwave Theory Tech. 47 (1999) 2059–2074.
[6] F.R. Yang, Y. Qian, R. Coccioli, T. Itoh, IEEE Microwave Guided Wave Lett. 8 (1998) 372–374.
[7] F.R. Yang, K.P. Ma, Y. Qian, T. Itoh, IEEE Trans. Microwave Theory Tech. 47 (1999) 1509–1514.
[8] F.R. Yang, K.P. Ma, Y. Qian, T. Itoh, IEEE Trans. Microwave Theory Tech. 47 (1999) 2092–2098.
[9] A. de Lustrac, F. Gadot, S. Cabaret, J.M. Lourtioz, T. Brillat, A. Priou, E. Akmansoy, Appl. Phys. Lett. 75 (1999) 1625–1627.
[10] J.-M. Lourtioz, A. de Lustrac, F. Gadot, S. Rowson, A. Chelnokov, T. Brillat, A. Ammouche, J. Danglot, O. Vanbésien, D. Lippens, IEEE J. Lightwave Technol. 17 (1999) 2025–2031.
[11] J.B. Pendry, A.J. Holden, D.J. Robbins, W.J. Stewart, IEEE Trans. Microwave Theory Tech. 47 (1999) 2075–2084.
[12] D.R. Smith, W.J. Padilla, D.C. Vier, S.C. Nemat-Nasser, S. Schultz, Phys. Rev. Lett. 84 (2000) 4184–4187.

[13] J.B. Pendry, Phys. Rev. Lett. 85 (1999) 3966–3969.
[14] K.M. Kulinowski, P. Jiang, H. Vaswani, V.L. Colvin, Adv. Mater. 12 (2000) 833.
[15] C. Cuisin, A. Chelnokov, J.-M. Lourtioz, D. Decanini, Y. Chen, J. Vac. Sci. Technol. B 18 (2000) 3505–3509.
[16] S.C. Kitson, W.L. Barnes, J.R. Sambles, Phys. Rev. Lett. 77 (1996) 2670–2673.
[17] W.L. Barnes, IEEE J. Lightwave Technol. 17 (1999) 2170–2182.
[18] V.A. Shubin, W. Kim, V.P. Safonov, A.K. Sarychev, R.L. Amstrong, V.M. Shalaev, IEEE J. Lightwave Technol. 17 (1999) 2183–2190;
F.J. Garcia-Vidal, J. Sanchez-Dehesa, A. Dechelette, E. Bustarret, T. Lopez-Rios, T. Fournier, B. Pannetier, IEEE J. Lightwave Technol. 17 (1999) 2191–2195.
[19] J.B. Pendry, A.J. Holden, W.J. Stewart, I. Youngs, Phys. Rev. Lett. 76 (1996) 4773.
[20] D.F. Sievenpiper, M.E. Sickmiller, E. Yablonovitch, Phys. Rev. Lett. 76 (1996) 2480.
[21] R. Ulrich, K.F. Renk, L. Genzel, IEEE Trans. Microwave Theory Tech. 11 (1963) 363–371.
[22] B. Lenoir, Thèse de doctorat de l'université de Limoges, Limoges, mars 2001.
[23] D.F. Sievenpiper, PhD thesis, University of California, 1999.
[24] Y. Qian, R. Coccioli, D.F. Sievenpiper, V. Radisic, E. Yablonovitch, T. Itoh, Microwave J. 1 (1999) 67–76.
[25] E.N. Economou, M.M. Sigalas, Phys. Rev. B 48 (1993) 13434–13438.
[26] T. Brillat, A. de Lustrac, F. Gadot, E. Akmansoy, J.-M. Lourtioz, in: Proc. PECS II Int. Workshop, Sendai, Japan, March 8–10, 2000, pp. T2–3.
[27] T. Brillat, Thèse de doctorat de l'université de Nanterre, Ville d'Avray, décembre 2000.
[28] G. Poilasne, P. Pouliguen, K. Mahdjoubi, Microwave Opt. Tech. Lett. 25 (2000) 36.
[29] V.G. Veselago, Usp. Fiz. Nauk 92 (1964) 517;
V.G. Veselago, Sov. Phys. – Usp. 10 (1968) 509.
[30] A. Scherer, J. Vuckovic, M. Loncar, T. Yoshie, O. Painter, D. Deppe, D. Dapkus, in: Proc. PECS III, St. Andrews, June, 2001.
[31] W.Y. Zhang, X.Y. Lei, Z.I. Wang, D.G. Zheng, W.Y. Tam, C.T. Chan, Ping Sheng, Phys. Rev. Lett. 84 (2000) 2853–2856.